ACS OMEGA

Open Access

http://pubs.acs.org/journal/acsodf

Article

Water Impact Dynamics and Mechanism Analysis of Polypropylene and Polypropylene/poly(ethylene-*co*-octene) Replica Surfaces with Nanowires under Low Temperature Conditions

Xing-Yu Wang* and Han-Xiong Huang

Cite This: *ACS Omega* 2024, 9, 33064−33071

Read Online

ACCESS | Metrics & More | Article Recommendations | Supporting Information

ABSTRACT: In this work, polypropylene (PP) and PP/poly(ethylene-*co*-octene) (PP/POE) blend replica surfaces with densely arranged nanowires are fabricated using a molding process. Morphology analysis shows that the nanowires on these replica surfaces have sharp tips and high aspect ratios. The droplet impact behaviors on the surfaces of the PP/POE blend replicas and PP replicas are investigated before and after freezing at −20 °C for 4 h. The height of the nanowires on the PP/POE blend replica surfaces is higher than that on the PP surface before and after freezing. The static wettability and droplet impact tests on the surfaces of PP/POE blend replicas and PP replica show that adding POE into the PP matrix can significantly increase the toughness of the nanowires on the PP/POE blend replica surfaces during the droplet impact at low temperatures. These investigations are favorable to broaden the practical applications of superhydrophobic surfaces in some severe environments.

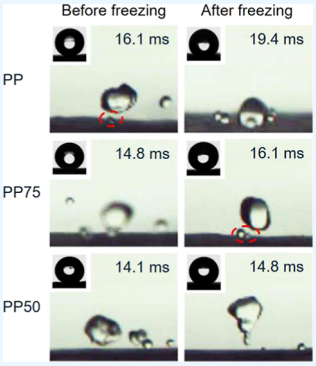

1. INTRODUCTION

Superhydrophobic polymer surfaces have been widely used in many fields, such as anti-icing,[1,2] self-cleaning,[3,4] drag-reduction,[5,6] and antiwetting.[7,8] In these applications, superhydrophobicity should be maintained during dynamic droplet impact. Meanwhile, it is important to investigate the stability of superhydrophobicity characteristics under various conditions, especially at subzero temperatures.[9,10] Therefore, it is a necessary and promising topic to easily prepare superhydrophobic polymer surfaces and investigate the dynamic impact of droplets on superhydrophobic surfaces.

Superhydrophobic surfaces with micro-/nanostructures can be prepared using several methods (such as injection molding,[4,11−13] hot embossing,[14,15] and casting or pouring[16,17]). The polymers used include polypropylene (PP), polyvinylidene fluoride, polystyrene, polydimethylsiloxane, and so on. Among these polymers, PP[18,19] is more used owing to its good mechanical and chemical properties, good processability, and low cost. However, the poor impact toughness of PP, especially at low temperatures, restricts its application in complex environments. The toughness of PP bulks can be significantly improved by adding rubbers or elastomers.[20−23] One of the most effective methods is to blend PP with poly(ethylene-*co*-octene) (POE) to prepare the PP/POE blends with good toughness, ductility, and high strength. The morphology, mechanical properties and rheological properties of the PP/POE blends have been examined in detail.[21,24,25] In addition, there are some research studies focused on the droplet impact behaviors on the PP/POE blend surfaces with nanohairs.[13,26] Huang et al.[26] prepared the PP/POE blend surfaces with nanohairs by injection molding and investigated the dynamic behavior of droplet impact on the replica surface at −10 °C. The results indicated that the nanohairs on the PP/POE blend surfaces have good flexibility and can shorten the contact time of the droplets. So far, less attention has been paid to the droplet impact on the blend replica surface with micro-/nanostructures after a period of exposure to a low temperature environment. Therefore, it is valuable to further explore the wetting properties and droplet impact behavior on the frozen PP/POE blend surfaces.

In this work, PP and PP/POE replicas with dense nanowires on their surfaces are prepared using a molding process. The morphology and height distributions of the nanowires on the replicas before and after freezing at −20 °C for 4 h are analyzed. The wettability and water droplet impact dynamic behavior on the replica surfaces before and after freezing are investigated. The contact angle (CA) and contact time of droplets on the replica surfaces are compared and analyzed. The low-temperature impact toughness improvement of the nanowires on the PP/POE blend replicas is analyzed.

Received: April 30, 2024
Revised: July 10, 2024
Accepted: July 12, 2024
Published: July 22, 2024

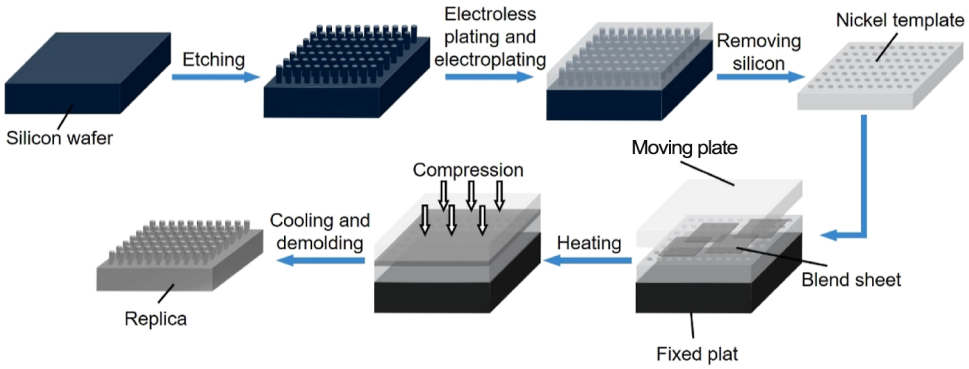

Figure 1. Schematics of the preparation process of replicas with nanowires on the surfaces.

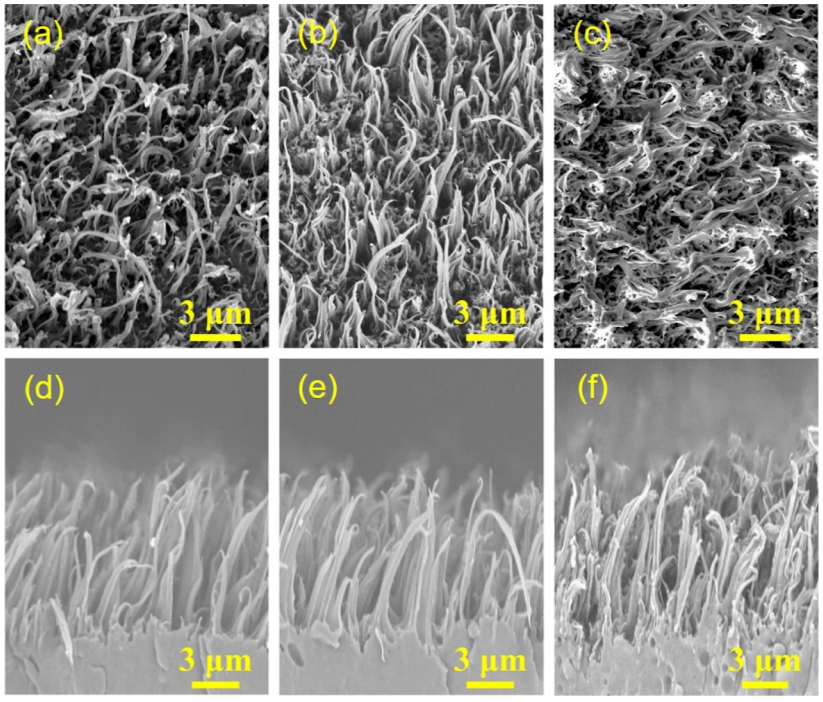

Figure 2. Surface [(a) PP, (b) PP75, and (c) PP50] and cross-section [(d) PP, (e) PP75, and (f) PP50] SEM images of the replica surfaces.

2. EXPERIMENTAL SECTION

2.1. Materials. Commercial PP (grade CJS700, China Petrochemical Co. Ltd.) and POE (Engage 8150, Dow Chemical Co. Ltd. USA) were used to prepare 0.77 mm thick PP/POE blend sheets using the injection compression molding process (for details, see Supporting Information, S1). The weight ratios of PP to POE were fixed at 75/25 and 50/50.

2.2. Preparation Process of Nanostructured Replicas. The preparation process of the PP and PP/POE replicas is shown in Figure 1. First, a silicon (Si) wafer substrate was prepared by chemical etching. Then, the nickel (Ni) template with a thickness of ∼220 μm was formed on the etched Si wafer by electroless plating and electroplating processes (for details, see Supporting Information, S2). The Ni template was fixed on the cavity surface of a compression molding mold. The prepared PP/POE blend sheet was placed on the Ni template and preheated at 230 °C for 3 min, followed by a compression process at 230 °C for 5 min. The compression pressure is 20 MPa. Finally, replicas with nanowires on their surfaces were obtained after cooling and demolding. The replicas molded from the PP and the PP/POE blends with weight ratios of 75/25 and 50/50 were denoted as PP, PP75, and PP50, respectively.

2.3. Characterization. The surface morphologies of the replicas were observed by scanning electron microscopy (SEM; Phenom Nano, Phenom Scientific, The Netherlands) at an accelerating voltage of 10 kV. The 3D morphology profile on the replicas was obtained by confocal microscopy (VK-X150 K, KEYENCE, Japan), and the heights and diameters of the nanowires were quantitatively analyzed by Nanomeasure Analysis software (Version 1.6). The CAs and roll-angles (RAs) of a water droplet (with a volume of 4 μL) on the replica surfaces were measured by an optical CA meter (OCA40, Data Physics Corporation, Germany). The CAs and RAs at five different locations on the replica surfaces were obtained, and the average values were calculated.

2.4. Droplet Impact Test. The droplet impact test devices mainly include a precision syringe pump and a high-speed camera (TS5, Fastec Imaging Co. USA) and a LED lamp (for details, see Supporting Information, Figure S3). The high-speed camera recorded the impact processes of the droplets at

https://doi.org/10.1021/acsomega.4c04128
ACS Omega 2024, 9, 33064−33071

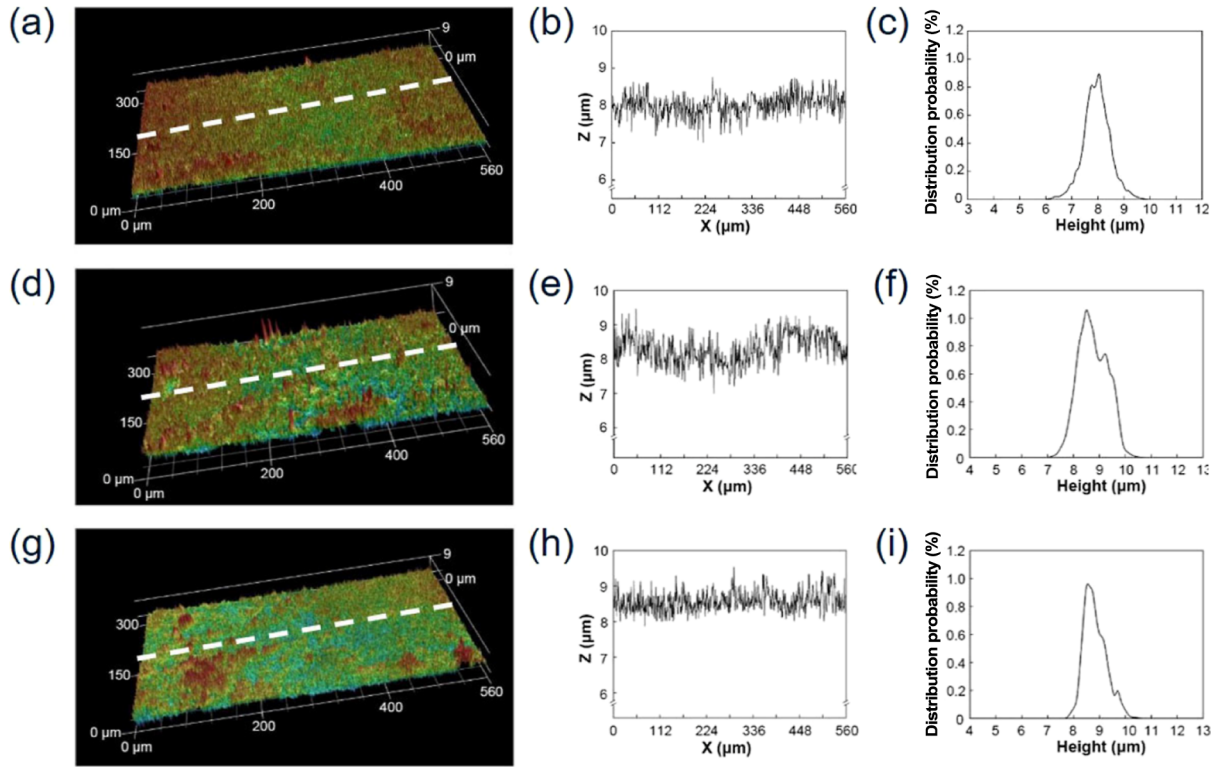

Figure 3. Surface morphology of the replica surfaces: 3D microscopy images [(a) PP, (d) PP75, and (g) PP50], cross-section profile curves of dashed lines [(b) PP, (e) PP75, and (h) PP50] in 3D microscope images, and nanowire height distributions [(c) PP, (f) PP75, and (i) PP50].

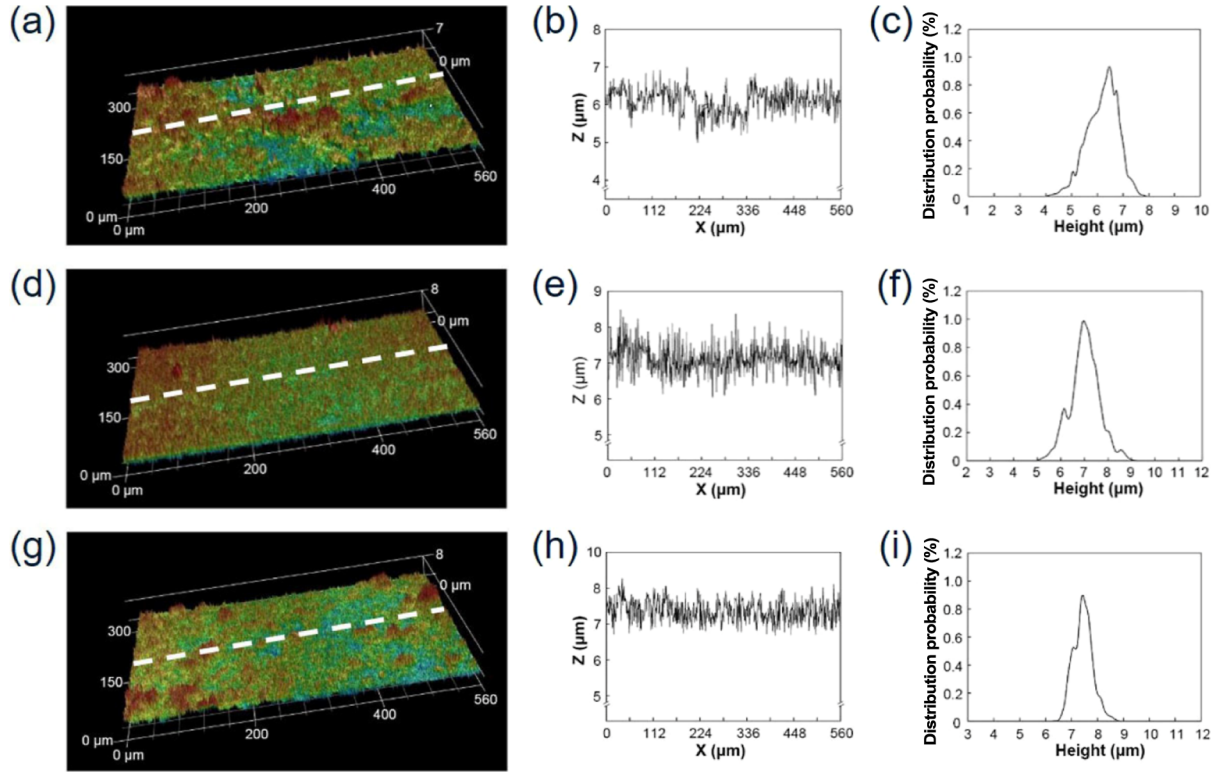

Figure 4. Surface morphology of the replica surfaces: 3D microscopy images [(a) PP, (d) PP75, and (g) PP50], cross-section profile curves of dashed lines [(b) PP, (e) PP75, and (h) PP50] in 3D microscope images, and nanowire height distributions [(c) PP, (f) PP75, and (i) PP50].

1500 fps. The replicas with a size of 20 × 20 × 0.15 mm were affixed on a glass plate. A water droplet with a diameter (D_0) of ∼3.0 mm was released from a syringe at different heights to obtain different droplet impact velocities (1.92 and 2.24 m/s). Droplet impact testing was carried out in two environments: room temperature and freezing conditions. It was conducted at

https://doi.org/10.1021/acsomega.4c04128
ACS Omega 2024, 9, 33064−33071

room temperature of 25 ± 1 °C with 60−70% relative humidity to evaluate the dynamic wettability on the replicas. Comparatively, it was conducted immediately after the replicas were frozen at −20 °C for 4 h and then taken out to evaluate the dynamic wettability.

3. RESULTS AND DISCUSSION

3.1. Morphology on Replica Surfaces. Figure 2 shows the surface and cross-section SEM images of the PP, PP75, and PP50 replicas. Figure 3 shows the 3D surface morphology, cross-section profile curves, and nanowires height distributions of these replicas. As can be seen in Figures 2 and 3, the nanowires with sharp tips are densely distributed on the replicas prepared by the molding process. The average diameters of the nanowires on the PP, PP75, and PP50 replicas are 277, 269, and 264 nm, and the corresponding heights are 8.1, 8.3, and 8.6 μm, respectively. These results indicate that the nanowires have a high aspect ratio.

Figure 4 shows the 3D surface morphology, cross-section profile curves, and nanowire height distributions of the frozen PP, PP75, and PP50 replicas, and the surface and cross-section SEM images of the frozen PP, PP75, and PP50 replicas are shown in Supporting Information, Figure S4. The average heights of the nanowires on these replica surfaces before and after freezing are listed in Table 1. Compared to the nanowires

Table 1. Average Heights of Nanowires on the PP, PP75, and PP50 Replicas

replica	before frozen (μm)	frozen for 4 h (μm)
PP	8.1	6.3
PP75	8.3	7.1
PP50	8.6	7.6

on the unfrozen ones, the average heights of nanowires on the frozen PP, PP75, and PP50 replica surfaces are shortened by 22.2, 14.5, and 11.6%, respectively. The shortening degrees of both replicas, especially the PP50 replica, are significantly smaller than that on the PP replica. These results suggest that adding the POE into the PP matrix can increase the low-temperature impact toughness of the nanowires, reducing the possibility of their fracture during freezing. The reason might be as follows: The Young's modulus and strength of the POE are much lower than those of the PP, the large deformation will be first formed for the POE phase under the load, then the voids or cavities forms at the phase interface, which can dissipate a large amount of impact energy so as to improve the impact toughness of the PP/POE blend replicas.[27,28]

3.2. Static Wettability on Replica Surfaces. The wettability of surfaces was closely related to their micro-/nano-structure with the CA being a significant metric for evaluating wettability,[29−32] and the CAs of water droplets on the PP, PP75, and PP50 replica surfaces are compared in Figure 5. The water droplets exhibit a spherical shape with high CAs of 152 ± 1.6, 155 ± 1.2, and 157 ± 1.1° on the PP, PP75, and PP50 replicas, respectively. In addition, all the water droplets on these replica surfaces show low RAs of <4° (for details, see Supporting Information, Video S1). This indicates that these replica surfaces exhibit superhydrophobicity and low adhesion characteristics. The reasons why the replicas derived from the PP/POE blends exhibit higher CAs than that on the PP replica are listed as follows. First, the PP75 and PP50 replicas have higher nanowire heights, more air pockets are

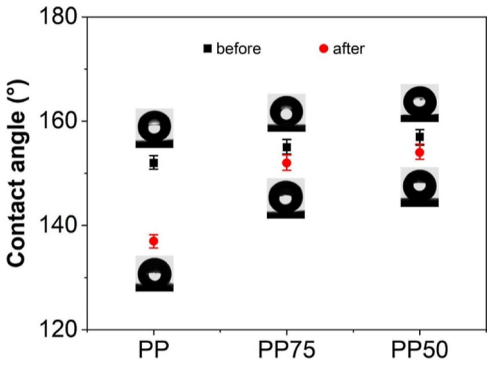

Figure 5. CA on PP, PP75, and PP50 replica surfaces before and after freezing.

trapped within the nanowires, which effectively prevents the droplets from penetrating into the nanowires.[11] Second, the added POE with a low surface energy characteristic can improve the superhydrophobicity of the replicas. The surface energies of the PP, PP75, and PP50 are 35.22, 32.97, and 28.24 mN/m, respectively.[33,34] After being frozen for 4 h, the CA of the PP replica is decreased from 152 to 137°, whereas the CAs for the PP75 and PP50 replicas are decreased slightly to 152 and 154° with high CA retention rates of 98.06 and 98.09%. The high CA retentions in the cases of PP75 and PP50 replicas demonstrate that the POE in the replicas can improve low-temperature toughness of the nanowires.

3.3. Droplet Impact on Replica Surfaces. Dynamic behavior of an impacting water droplet is another way to characterize the surface wettability and the adhesive characteristics between water droplet and solid surface.[35] Figure 6 shows the typical snapshots of droplets with the velocity of 1.92 m/s impacting on the PP, PP75, and PP50 replica surfaces (for sample test, see Video S2). The process of the droplet impact can be divided into three stages: spreading, retracting, and rebounding. When the droplet contacts the replica surface, the droplet starts to spread outward and become "flat" under the influence of kinetic energy that is partially converted into the surface energy of the droplet, and the other part is converted into viscous dissipation energy. When the droplet reaches the maximum spreading diameter (D_{max}) at the end of the spreading stage, it begins to retract under the surface tension and the contact area between the droplet and the surface decreases. Finally, the droplet rebounds from the replica surface. All the PP, PP75, and PP50 replica surfaces exhibit the same spreading time of ∼3.5 ms. At the retracting stage, the PP replica has a much longer contact time of 16.1 ms than those of PP75 (14.8 ms) and PP50 (14.1 ms) replicas. The addition of POE improves the impact toughness of the PP/POE replica, reducing the possibility of nanowire fracture under low temperature. The relatively higher nanowires can have more air pockets between the droplet and nanowires, effectively preventing droplet penetration and shortening contact time to a certain extent. In addition, the addition of POE can improve the elasticity of PP/POE replicas, which means that the replica surface can absorb energy during droplet impact and promote droplet detachment during energy release. This elastic behavior can reduce the contact time between the droplet and the substrate as it provides additional energy to overcome the adhesion between the droplet and the surface. Moreover, more small droplets are generated on the surface with high content of POE after impacting, these small droplets will carry away

https://doi.org/10.1021/acsomega.4c04128
ACS Omega 2024, 9, 33064−33071

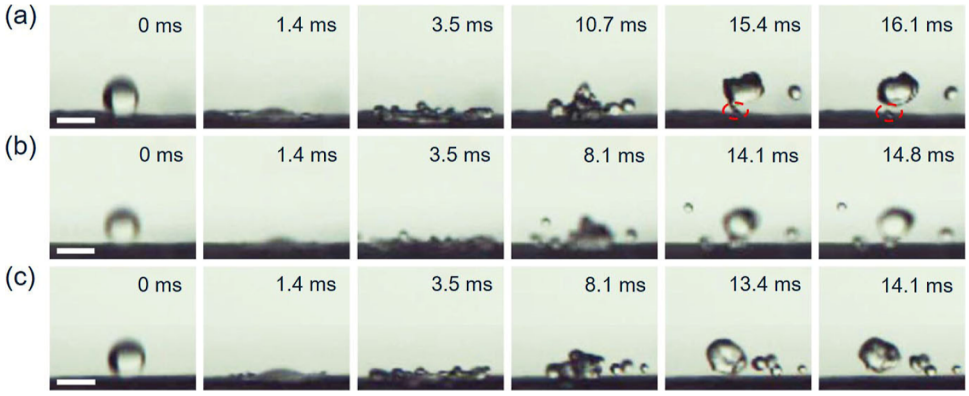

Figure 6. Typical snapshots of droplets (D_0 = 3.0 mm) with the velocity of 1.92 m/s impacting on the (a) PP, (b) PP75, and (c) PP50 replica surfaces at room temperature (scale bar: 3 mm).

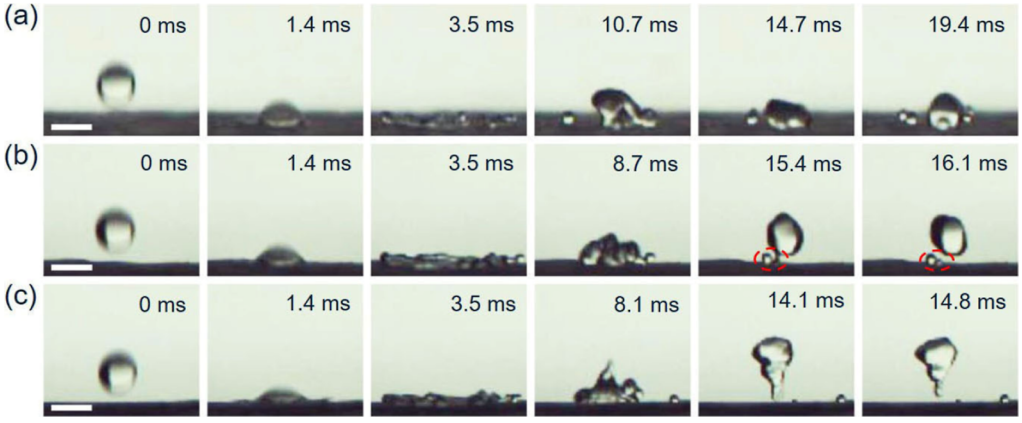

Figure 7. Typical snapshots of droplets (D_0 = 3.0 mm) with the velocity of 1.92 m/s impacting on the frozen (a) PP, (b) PP75, and (c) PP50 replica surfaces (scale bar: 3 mm).

more energy, which will increase energy loss during the droplet impact, and these small droplets may exhibit different detachment behaviors, which can also affect the contact time. In other words, the addition of POE will shorten the contact time on the surface under the influence of the above factors.

Figure 7 shows the typical snapshots of droplets with a velocity of 1.92 m/s impacting the frozen PP, PP75, and PP50 replica surfaces (for sample test, see Video S2). As shown in Figure 7a, compared to the unfrozen one, the droplet impacting the frozen PP replica surface cannot rebound after the spreading and retracting stages and finally is pinned on the frozen PP replica surface. This may lead to some problems in practical applications, such as contamination and freezing on the frozen PP surface. However, the droplet impacting the frozen PP75 and PP50 replica surfaces can rebound after the spreading and retracting stages (Figure 7b,c). These results demonstrate that the frozen PP and PP/POE replica surfaces exhibit totally different droplet impact behaviors and that the droplet can rebound from the PP/POE replica surfaces. In addition, the contact time on the PP75 surface is 8.8% longer than that on the PP50 surface. This indicates that the adding of more POE can improve the impact toughness of the PP/POE blend replicas and shorten the contact time.

Figure 8 shows the typical snapshots of droplets with the velocity of 2.24 m/s impacting the PP, PP75, and PP50 replica surfaces before and after freezing (for sample test, see Video S3). As shown in Figure 8a, when the droplet contacts the PP replica surface, it spreads and finally is pinned on the surface. In the cases of the PP75 and PP50 replica surfaces (Figure 8b,c), the droplets can rebound from the surfaces. In addition, the contact time on the PP75 replica surface is 4.05% longer than that on the PP50 surface. After these replicas are frozen for 4 h, the droplet impacting the frozen PP replica surface cannot rebound after the spreading and retracting stages (Figure 8d). For the frozen PP75 and PP50 replicas (Figures 8e,f), the droplets can still rebound from the surfaces. In addition, the contact time on the PP75 replica surface is 8.07% longer than that on the PP50 surface. The added POE has a great influence on the droplet impact process on the replica surface, with the PP/POE blend replicas exhibiting impact toughness and dynamic hydrophobicity.

The different droplet impact behaviors between the PP/POE and PP replicas can be explained as follows. For the PP replica, the nanowires on the surface have a weak impact toughness. After being impacted by droplets at a lower velocity, the possibility of nanowire fracture is relatively low. The air pocket trapped within the nanowires can prevent the penetration of droplets. Therefore, the droplet can rebound from the surface. When the replica is frozen for 4 h or the droplet impact velocity increases, the possibility of nanowire fracture increases and the heights of nanowires significantly decrease. Since the solid−liquid−air interface and capillary pressure decrease, these air pockets cannot effectively prevent the penetration of the droplet. Finally, the droplet is pinned on the PP replica. For the PP/POE replicas, the toughness of the nanowires increases due to the high toughness of POE.[28] After

https://doi.org/10.1021/acsomega.4c04128
ACS Omega 2024, 9, 33064−33071

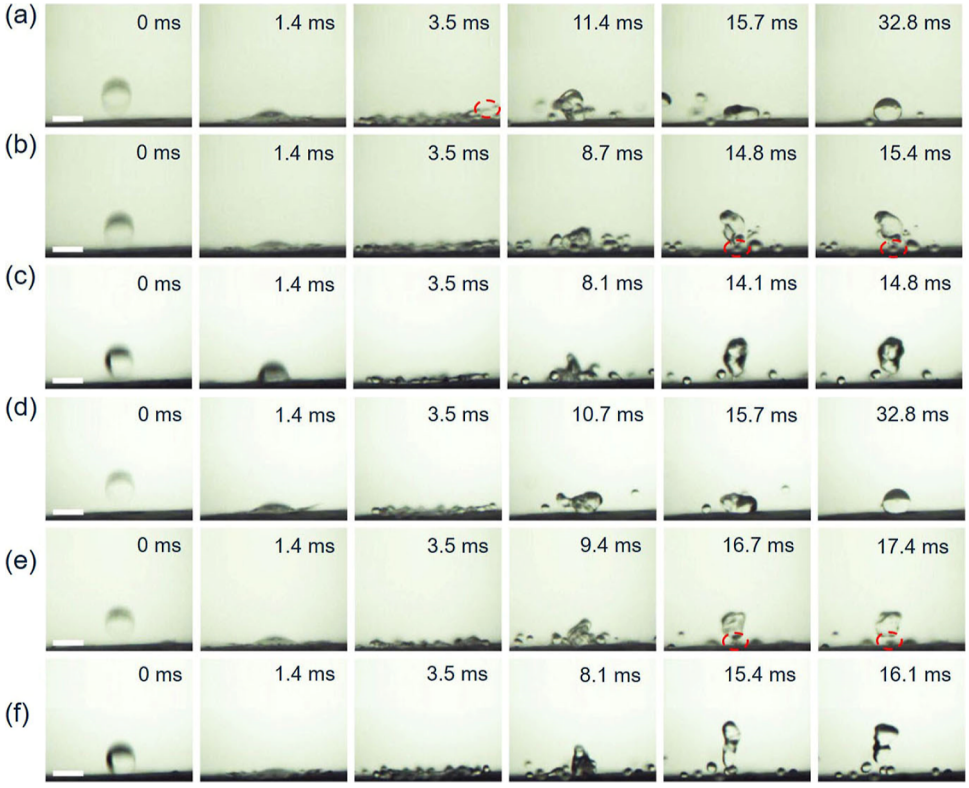

Figure 8. Typical snapshots of droplets (D_0 = 3.0 mm) with the velocity of 2.24 m/s impacting on the unfrozen [(a) PP, (b) PP75, and (c) PP50] and frozen [(d) PP, (e) PP75, and (f) PP50] replica surfaces (scale bar: 3 mm).

being impacted by droplets, the possibility of nanowire fracture on the PP/POE surface is lower than that on the PP surface, reducing the possibility of the droplet being pinned on the surface. When the replicas are frozen for 4 h, the height of the nanowires exhibit obviously smaller shortening degrees, and these nanowires have an enhanced low-temperature impact toughness. These nanowires play an important role in improving hydrophobicity and especially reducing the droplet adhesion. The air pockets trapped within the nanowires can be retained and prevent the penetration of droplets. Finally, the droplet can rebound from the blend replica.

4. CONCLUSIONS

In this work, the PP, PP75, and PP50 replicas with high-aspect-ratio nanowires on their surfaces were fabricated based on a molding process. The morphologies of the PP, PP75, and PP50 replica surfaces demonstrate that the average heights of the nanowires on the PP/POE blend replica surfaces are higher than that on the PP replica surface. The CAs on the PP and PP/POE blend replica surfaces are >150°. After freezing for 4 h, the average heights of nanowires on the PP75 and PP50 replica surfaces is still higher than that on the PP surface. The wetting characteristics on the PP replica surface changes from superhydrophobicity to hydrophobicity, while the PP/POE replica surfaces still show superhydrophobicity. The PP and PP/POE replica surfaces exhibit totally different droplet impact behaviors at the velocity of 2.24 m/s. The droplets can rebound from the PP/POE replicas, while the droplet is pinned on the PP replica at the velocity of 2.24 m/s. Both the replicas exhibit good dynamic superhydrophobic stability, and the contact time on PP50 replica surface is shorter than that on the PP75 replica surface. The results show that the adding of POE into PP matrix can effectively increase the low temperature impact toughness of nanowires. This research is expected to broaden the practical applications of superhydrophobic surfaces in some severe environments.

■ ASSOCIATED CONTENT

Supporting Information

The Supporting Information is available free of charge at https://pubs.acs.org/doi/10.1021/acsomega.4c04128.

Preparation process of PP/POE blends sheet, preparation of the Ni template, surface SEM images of the etched Si wafer and Ni template, and schematics of droplet impact (PDF)

Dynamic rolling processes of water droplet on the replica surfaces (MOV)

Droplet impact with the velocity of 1.92 m/s impacting on the PP, PP75, and PP50 replica surfaces before and after freezing (MOV)

Droplet impact with the velocity of 2.24 m/s impacting on the PP, PP75, and PP50 replica surfaces before and after freezing (MOV)

■ AUTHOR INFORMATION

Corresponding Author

Xing-Yu Wang − *Lab for Micro Molding and Polymer Rheology, Guangdong Provincial Key Laboratory of Technique and Equipment for Macromolecular Advanced Manufacturing, South China University of Technology, Guangzhou 510640, P. R. China;* orcid.org/0009-0009-0846-1841; Email: 1437751926@qq.com

https://doi.org/10.1021/acsomega.4c04128
ACS Omega 2024, 9, 33064−33071

Author

Han-Xiong Huang − *Lab for Micro Molding and Polymer Rheology, Guangdong Provincial Key Laboratory of Technique and Equipment for Macromolecular Advanced Manufacturing, South China University of Technology, Guangzhou 510640, P. R. China;* orcid.org/0000-0001-8805-3040

Complete contact information is available at: https://pubs.acs.org/10.1021/acsomega.4c04128

Notes

The authors declare no competing financial interest.

■ ACKNOWLEDGMENTS

Financial support provided by the National Natural Science Foundation of China (Grant 51533003) and the Guangzhou Science and Technology Project (grant 201807010088) is gratefully acknowledged. The experiments in this work were carried out in the Guangdong Provincial Key Laboratory of Technique and Equipment for Macromolecular Advanced Manufacturing. The author is grateful to H.-X.H. for providing all necessary guidance to carry out this work. The author would also like to sincerely thank Wei Yuan, Guo Jiang, and Xiao-Qing Zhang for their help.

■ REFERENCES

(1) Korczeniewski, E.; Bryk, P.; Koter, S.; Kowalczyk, P.; Zięba, M.; Łępicka, M.; Kurzydłowski, K. J.; Markiewicz, K. H.; Wilczewska, A. Z.; Kujawski, W.; Boncel, S.; Al-Gharabli, S.; Świdziński, M.; Smoliński, D. J.; Kaneko, K.; Kujawa, J.; Terzyk, A. P. Are Nanohedgehogs Thirsty? Toward New Superhydrophobic and Anti-icing Carbon Nanohorn-Polymer Hybrid Surfaces. *Chem. Eng. J.* **2022**, *446*, 137126.

(2) Idriss, H.; Guselnikova, O.; Postnikov, P.; Kolska, Z.; Haušild, P.; Čech, J.; Lyutakov, O.; Švorčík, V. Versatile and Scalable Icephobization of Airspace Composite by Surface Morphology and Chemistry Tuning. *ACS Appl. Polym. Mater.* **2020**, *2*, 977−986.

(3) Han, Z. W.; Wang, Z.; Li, B.; Feng, X. M.; Jiao, Z. B.; Zhang, J. Q.; Zhao, J.; Niu, S. C.; Ren, L. Q. Flexible Self-Cleaning Broadband Antireflective Film Inspired by the Transparent Cicada Wings. *ACS Appl. Mater. Interfaces* **2019**, *11*, 17019−17027.

(4) Guan, W. S.; Huang, H. X.; Chen, A. F. Tuning 3D Topography on Biomimetic Surface for Efficient Self-cleaning and Microfluidic Manipulation. *J. Manuf. Syst.* **2015**, *25*, 035001.

(5) Zhu, Y.; Yang, F. C.; Guo, Z. G. Bioinspired Surfaces with Special Micro-structures and Wettability for Drag Reduction: Which Surface Design Will Be a Better Choice? *Nanoscale* **2021**, *13*, 3463−3482.

(6) Bixler, G. D.; Bhushan, B. Fluid Drag Reduction and Efficient Self-cleaning with Rice Leaf and Butterfly Wing Bioinspired Surfaces. *Nanoscale* **2013**, *5*, 7685−7710.

(7) Li, X. Y.; Li, Y. P.; Huo, L.; Lei, M. K. Effect of Au Film Mask on Antiwetting and Antireflection Properties of Nanostructural Polymer by Plasma Nanotexturing. *Surf. Topogr.: Metrol. Prop.* **2022**, *10*, 035023.

(8) Lee, W. L.; Wang, D.; Wu, J.; Ge, Q.; Low, H. Y. Injection Molding of Superhydrophobic Submicrometer Surface Topography on Macroscopically Curved Objects: Experimental and Simulation Studies. *ACS Appl. Polym. Mater.* **2019**, *1*, 1547−1558.

(9) Wang, H.; Wu, Q.; Okagaki, J.; Alizadeh, A.; Shamim, J. A.; Hsu, W. L.; Daiguji, H. Bouncing Behavior of a Water Droplet on a Superhydrophobic Surface near Freezing Temperatures. *Int. J. Heat Mass Transfer* **2021**, *174*, 121304.

(10) Wang, Y. Y.; Liu, J.; Li, M. Z.; Wang, Q. J.; Chen, Q. M. The Icephobicity Comparison of Polysiloxane Modified Hydrophobic and Superhydrophobic Surfaces under Condensing Environments. *Appl. Surf. Sci.* **2016**, *385*, 472−480.

(11) Huang, H. X.; Wang, X. Biomimetic Fabrication of Micro-/nanostructure on Polypropylene Surfaces with High Dynamic Superhydrophobic Stability. *Mater. Today Commun.* **2019**, *19*, 487−494.

(12) Zhou, M. Y.; Xiong, X.; Jiang, B. Y.; Weng, C. Fabrication of High Aspect Ratio Nanopillars and Micro/nano Combined Structures with Hydrophobic Surface Characteristics by Injection Molding. *Appl. Surf. Sci.* **2018**, *427*, 854−860.

(13) Huang, H. X.; Huang, H. L. Shortening Droplet Contact Time over a Wider Impact Velocity Range by Molding Flexible Nanohairs and Substrates. *ACS Appl. Polym. Mater.* **2021**, *3*, 5749−5757.

(14) Mulroney, A. T.; Gupta, M. C. Optically Transparent Superhydrophobic Polydimethylsiloxane by Periodic Surface Microtexture. *Surf. Coat. Technol.* **2017**, *325*, 308−317.

(15) Roslizar, A.; Dottermusch, S.; Füllers, F.; Kavalenka, M. N.; Guttmann, M.; Schneider, M.; Paetzold, U. W.; Hölscher, H.; Richards, B. S.; Klampaftis, E. Self-cleaning Performance of Superhydrophobic Hot-embossed Fluoropolymer Films for Photovoltaic Modules. *Sol. Energy Mater. Sol. Cells* **2019**, *189*, 188−196.

(16) Kang, B. C.; Sung, J.; So, H. Y. Realization of Superhydrophobic Surfaces Based on Three-Dimensional Printing Technology. *Int. J. Precis. Eng. Manuf. - Green Technol.* **2021**, *8*, 47−55.

(17) Kim, B. C.; Lim, D. W.; Kim, J. H.; Lee, H. T. Superhydrophobicity and Corrosion Resistance of AISI 4140 Mold Made through Nanosecond Laser Texturing. *Int. J. Adv. Manuf. Technol.* **2022**, *119*, 5119−5130.

(18) Li, Y. P.; Li, X. Y.; Liu, X.; Zhu, B.; Muzammil, I.; Lei, M. K.; Lakhtakia, A. Biomimetic Random Arrays of Nanopillars and Nanocones with Robust Antiwetting Characteristics. *J. Phys. Chem. C* **2020**, *124*, 17095−17102.

(19) Brown, P. S.; Bhushan, B. Durable Superoleophobic Polypropylene Surfaces. *Philos. Trans. R. Soc., A* **2016**, *374*, 20160193.

(20) Xia, Y.; Ren, Q. L.; Zhang, F. F.; Zhang, W. M.; Guo, J.; Zhang, S. Study on the Toughening Mechanism of PP/EVA Dynamically Crosslinked Blend. *J. Macromol. Sci., Part A: Pure Appl.Chem.* **2016**, *53*, 523−529.

(21) Kim, D. K.; Lee, S. H.; Hong, S. K.; Han, S. W.; Lee, D. H.; Yu, S. Low-Temperature-Toughened Polypropylene Blends with Highly Packed Elastomeric Domains. *ACS Appl. Polym. Mater.* **2022**, *4*, 7834−7840.

(22) Shangguan, Y. G.; Chen, F.; Yang, J.; Jia, E. W.; Zheng, Q. A new Approach to Fabricate Polypropylene Alloy with Excellent Low-temperature Toughness and Balanced Toughness-rigidity through Unmatched Thermal Expansion Coefficients between Components. *Polymer* **2017**, *112*, 318−324.

(23) Zhang, B.; Zhong, W. T.; Fu, Z. S.; Fan, Z. Q. Polyethylene/crystalline Ethylene-propylene Copolymer/amorphous Ethylene-propylene Copolymer in-reactor Alloys Synthesized by Periodic Switching Polymerization Process: An Excellent Toughener for Polypropylene. *Eur. Polym. J.* **2021**, *154*, 110563.

(24) Wang, J. F.; Yang, M. T.; Wu, H.; Guo, S. Y. Mechanically Strong and Ductile Polypropylene/Poly(ethylene-*co*-octene) Blends Prepared Through Multistretched Extrusion: Morphological Evolution, Toughening, and Reinforcing Mechanism. *Polym.-Plast. Technol. Mater.* **2018**, *57*, 417−428.

(25) Wang, J. F.; Wang, C. L.; Zhang, X. L.; Wu, H.; Guo, S. Y. Morphological Evolution and Toughening Mechanism of Polypropylene and Polypropylene/poly(ethylene-*co*-octene) Alternating Multilayered Materials with Enhanced Low-temperature Toughness. *RSC Adv.* **2014**, *4*, 20297−20307.

(26) Huang, H. X.; Huang, H. L. Low-temperature Impact Behavior of Droplet on Injection-compression Molded Nanostructured PP/POE Blend Surfaces. *Chem. J. Chin. Univ.* **2021**, *42*, 3195−3202.

(27) Huang, H. X.; Li, W. P. Revealing Toughening Mechanism for Alternating Multilayered Polypropylene/poly(ethylene-*co*-octene) Sheets. *Polym. Test.* **2015**, *41*, 245−251.

(28) Chen, A. F.; Lai, J. D.; Li, M. K.; Fang, C. K.; Qin, G. F.; Ding, S.; Zhang, J. J.; Zhang, Z. R.; Huang, H. X. Long-Lived T-Shaped Micropillars with Submicron-Villi on PP/POE Surfaces with Grinding-Enhanced Water Repellency Fabricated via Hot Compression Molding. *J. Phys. Chem. B* **2021**, *125*, 7290−7298.
(29) Xiong, Z.; Yu, H. Y.; Gong, X. Designing Photothermal Superhydrophobic PET Fabrics via In Situ Polymerization and 1,4-Conjugation Addition Reaction. *Langmuir* **2022**, *38*, 8708−8718.
(30) Yu, H. Y.; Wu, M.; Duan, G. G.; Gong, X. One-step Fabrication of Eco-friendly Superhydrophobic Fabrics for High-efficiency Oil/water Separation and Oil Spill Cleanup. *Nanoscale* **2022**, *14*, 1296−1309.
(31) Wu, T.; Xu, W. H.; Guo, K.; Xie, H.; Qu, J. P. Efficient Fabrication of Lightweight Polyethylene Foam with Robust and Durable Superhydrophobicity for Self-cleaning and Anti-icing Applications. *Chem. Eng. J.* **2021**, *407*, 127100.
(32) Zhang, Y. Y.; Gong, X. Smart and Durable pH-responsive Superhydrophobic Fabrics with Switchable Surface Wettability for High-efficiency and Complex Oil/water Separation. *Giant* **2023**, *14*, 100157.
(33) Kahl, C.; Gemmeke, N.; Bagnucki, J.; Heim, H. P. Investigations on Fiber-matrix Properties of Heat-treated and UV-treated Regenerated Cellulose Fibers. *Composites, Part A* **2022**, *152*, 106669.
(34) Píchal, J.; Cerman, J.; Šourková, H.; Špatenka, P. Plasma Pretreatment of Polypropylene Surface for Industrial Purposes. *Mater. Manuf. Process* **2022**, *37*, 1483−1489.
(35) Yang, C. J.; Chao, J. Q.; Zhang, J. C.; Zhang, Z. T.; Liu, X.; Tian, Y. L.; Zhang, D. W.; Chen, F. Z. Functionalized CFRP Surface with Water-repellence, Self-cleaning and Anti-icing Properties. *Colloids Surf., A* **2020**, *586*, 124278.

https://doi.org/10.1021/acsomega.4c04128
ACS Omega 2024, 9, 33064−33071